frontiers in Climate

TYPE Original Research
PUBLISHED 13 April 2026
DOI 10.3389/fclim.2026.1801667

OPEN ACCESS

EDITED BY
Hyacinth Nnamchi,
Helmholtz Association of German Research Centres (HZ), Germany

REVIEWED BY
Simi Mathew,
Indian Institute of Technology Madras, India
C. V. Naidu,
Andhra University, India

*CORRESPONDENCE
Ligin Joseph
✉ l.joseph@soton.ac.uk

RECEIVED 01 February 2026
REVISED 16 March 2026
ACCEPTED 19 March 2026
PUBLISHED 13 April 2026

CITATION
Joseph L, Skliris N, Vishnu S, Dey D and Marsh R (2026) Drivers and variability of marine heatwaves in the North Indian Ocean and their impacts on South Asian monsoon rainfall.
Front. Clim. 8:1801667.
doi: 10.3389/fclim.2026.1801667

Drivers and variability of marine heatwaves in the North Indian Ocean and their impacts on South Asian monsoon rainfall

Ligin Joseph[1]*, Nikolaos Skliris[1], S. Vishnu[2], Dipanjan Dey[1,3] and Robert Marsh[1]

[1]School of Ocean and Earth Science, University of Southampton, Southampton, United Kingdom, [2]School of Earth, Environmental and Sustainability Sciences, Indian Institute of Science Education and Research, Thiruvananthapuram, India, [3]School of Earth, Ocean and Climate Sciences, Indian Institute of Technology Bhubaneswar, Khordha, India

Our planet is warming rapidly, accompanied by an increase in the frequency and intensity of marine heatwaves (MHWs). Beyond their impacts on marine ecosystems, MHWs can also modulate regional climate systems, including the Asian monsoon. Here, we investigate the variability, drivers, and monsoon impacts of MHWs in the North Indian Ocean using detrended sea surface temperature anomalies over the period 1982–2024. An Empirical Orthogonal Function (EOF) analysis of MHW intensity identifies two leading modes of variability. The first mode (PC1), explaining 22% of the variance, is characterized by basin-wide MHWs with enhanced intensity in the Arabian Sea and is associated with weakened monsoon winds, reduced evaporation and cloud cover, and enhanced shortwave radiation, leading to upper-ocean warming. The second mode (PC2), accounting for 8% of the variance, exhibits a dipole structure, with intensified MHWs in the Bay of Bengal and suppressed activity in the Arabian Sea during its positive phase, and the opposite pattern during its negative phase. Large-scale climate modes modulate these patterns. Basin-wide MHWs resembling PC1 are usually associated with the mature phase of El Niño, coinciding with the transition from active to break phases of the Monsoon Intraseasonal Oscillation (MISO). Under similar MISO conditions, La Niña tends to favor $PC2^{+}$-type warming. These modes are accompanied by distinct rainfall responses: PC1 and $PC2^{+}$ are linked to wetter conditions over southern India and drier conditions in the north, whereas $PC2^{-}$ corresponds to more widespread dryness. The termination of MHWs is associated with the re-intensification of monsoon winds, which both suppresses further ocean warming and enhances rainfall through increased evaporation and moisture transport. Together, these results point to a potential interaction between MHWs, monsoon intraseasonal variability, and ENSO and suggest that certain climate conditions may favor the transition of MISO-related ocean warming into marine heatwaves, with implications for monsoon predictability in a warming climate.

KEYWORDS
ENSO, Indian Ocean, Indian Ocean warming, marine heatwaves, Monsoon Intraseasonal Oscillation

1 Introduction

Our planet is warming at an unprecedented rate, and 2024 was recorded as the hottest year on record for both land and ocean temperatures (Rohde, 2025; World Meteorological Organization, 2025). The rise in ocean temperature has gained increasing scientific attention due to its far-reaching implications for the climate system and the intensification of extreme weather events (Johnson et al., 2023). Among the world's oceans, the Indian Ocean is warming the fastest, making it a critical region for understanding ocean-atmosphere interactions in a warming world (Roxy et al., 2014; Venegas et al., 2023).

The Indian Ocean is the principal source of moisture for the South Asian Monsoon, which is the largest monsoon system, on which millions of people depend for agriculture, water security, and livelihoods (Dey and Döös, 2021). Any change in the Indian Ocean's thermal structure, therefore, has the potential to substantially influence monsoon variability and intensity (Roxy et al., 2015; Yadav and Roxy, 2019; Skliris et al., 2022; Joseph et al., 2024). While previous studies have focused on the mean-state warming of the Indian Ocean, particularly the western basin including the Arabian Sea (Oppo and Rosenthal, 2010; Swapna et al., 2013; Roxy et al., 2014; D'Mello and Kumar, 2018; Pratik et al., 2018; Zhang Y. et al., 2018; Mathew et al., 2018; McMonigal et al., 2022; Albert et al., 2023; Nisha et al., 2023; Shee et al., 2023; Sajidh et al., 2026; Joseph et al., 2026), relatively limited attention has been paid to understanding periods of anomalously high Sea Surface Temperature (SST) lasting days to weeks, known as marine heatwaves (MHWs).

Recent studies suggest that MHWs are becoming more frequent, more intense, and longer in duration across various regions of the global ocean, driven by anthropogenic warming and internal climate variability (Oliver et al., 2018; Saranya et al., 2022; Chatterjee et al., 2022; Chakraborty et al., 2023; Cheng et al., 2023; Koul et al., 2023; Capotondi et al., 2024; Gupta et al., 2024). Saranya et al. (2022) demonstrated that the frequency of MHWs in the western Indian Ocean and northern Bay of Bengal is increasing, often in association with background ocean warming and El Niño events. These MHWs, in turn, influence Indian summer monsoon rainfall patterns by suppressing rainfall over central India and enhancing it over the south, depending on the location of the MHW. Similarly, Chatterjee et al. (2022) found an increasing trend in MHW events over the northern Arabian Sea linked to increasing mean SST and El Niño forcing. Chakraborty et al. (2023) showed that MHW intensity is higher in the western Arabian Sea than in the east and that these events significantly influence biogeochemical cycles. Liang et al. (2024) found high correlations between the Indian Ocean Dipole (IOD) and MHW days in the Bay of Bengal. Kumar et al. (2023) documented that the MHWs in the Bay of Bengal are driven by changes in the net heat flux and anticyclonic eddies. Furthermore, Gupta et al. (2023) showed that the surface MHWs in the Bay of Bengal are frequent during El Niño and positive IOD years, whereas subsurface MHWs are usually driven by the thermocline changes driven by La Niña and negative IOD.

Collectively, these studies affirm that MHWs in the North Indian Ocean are intensifying, although they differ in regional focus and metrics. Importantly, all these studies use a fixed baseline seasonal climatology to define MHWs, which can mix long-term ocean warming with short-term events. This makes MHWs appear more frequent in recent decades and could even lead to scenarios where oceans enter a "permanent MHW state," particularly in rapidly warming regions like the Indian Ocean. Indeed, recent projections suggest the Indian Ocean could permanently exceed MHW thresholds by 2050 under fixed-baseline definitions (Roxy et al., 2024). To address this, several studies have proposed defining MHWs using detrended SST anomalies or a moving baseline, which helps distinguish true marine heatwave events from long-term warming (Jacox, 2019; Rosselló et al., 2023; Amaya et al., 2023; Capotondi et al., 2024). A recent study suggests reserving the term "Marine Heatwaves" for events identified using a moving baseline approach, while using "long-term temperature trend" for slow changes in the ocean temperature and using "total heat exposure" to describe the combination of long-term warming and marine heatwaves (Amaya et al., 2023). This avoids the misclassification of slowly increasing background SST as MHWs.

Despite the emergence of improved methodologies, the use of detrended or moving-baseline approaches in defining MHWs in the North Indian Ocean remains limited. Moreover, no comprehensive study has yet examined the variability, drivers, and monsoonal consequences of these events in this climate-sensitive basin. This study fills that critical gap. In this present study, we apply a detrended SST anomaly framework to identify MHWs in the North Indian Ocean, allowing us to disentangle short-term marine heatwave dynamics from the long-term warming signal. Building on this improved detection, we conduct a detailed investigation into the dominant modes of MHW variability, diagnose their physical drivers, including oceanic and atmospheric forcing mechanisms, and investigate their possible impacts on the monsoon rainfall over South Asia. By bridging marine heat extremes and monsoonal variability, our study offers a new understanding of how upper-ocean thermal anomalies influence regional climate, with implications for prediction and climate risk assessment across South Asia.

2 Data and methods

2.1 Data used

To identify MHWs and investigate their drivers in the North Indian Ocean, we use daily SST and atmospheric variables including 10-meter winds, mean sea level pressure (MSLP), surface latent heat flux, net shortwave radiation at the surface, total cloud cover, total precipitation, and vertically integrated water vapor flux from the ERA5 reanalysis dataset (Hersbach et al., 2020). The ERA5 SST is based on HadISST2 from 1979 to August 2007 and on OSTIA from September 2007 onward, benefiting from rigorous data assimilation (Titchner and Rayner, 2014; Good et al., 2020; Hersbach et al., 2020). We use ERA5 SST to identify MHW events and analyze their drivers to ensure consistency with the atmospheric fields, all of which are derived from ERA5. In addition, we compute the MHW characteristics (e.g., frequency, duration and intensity; see Figure 1) using NOAA OISST to take advantage

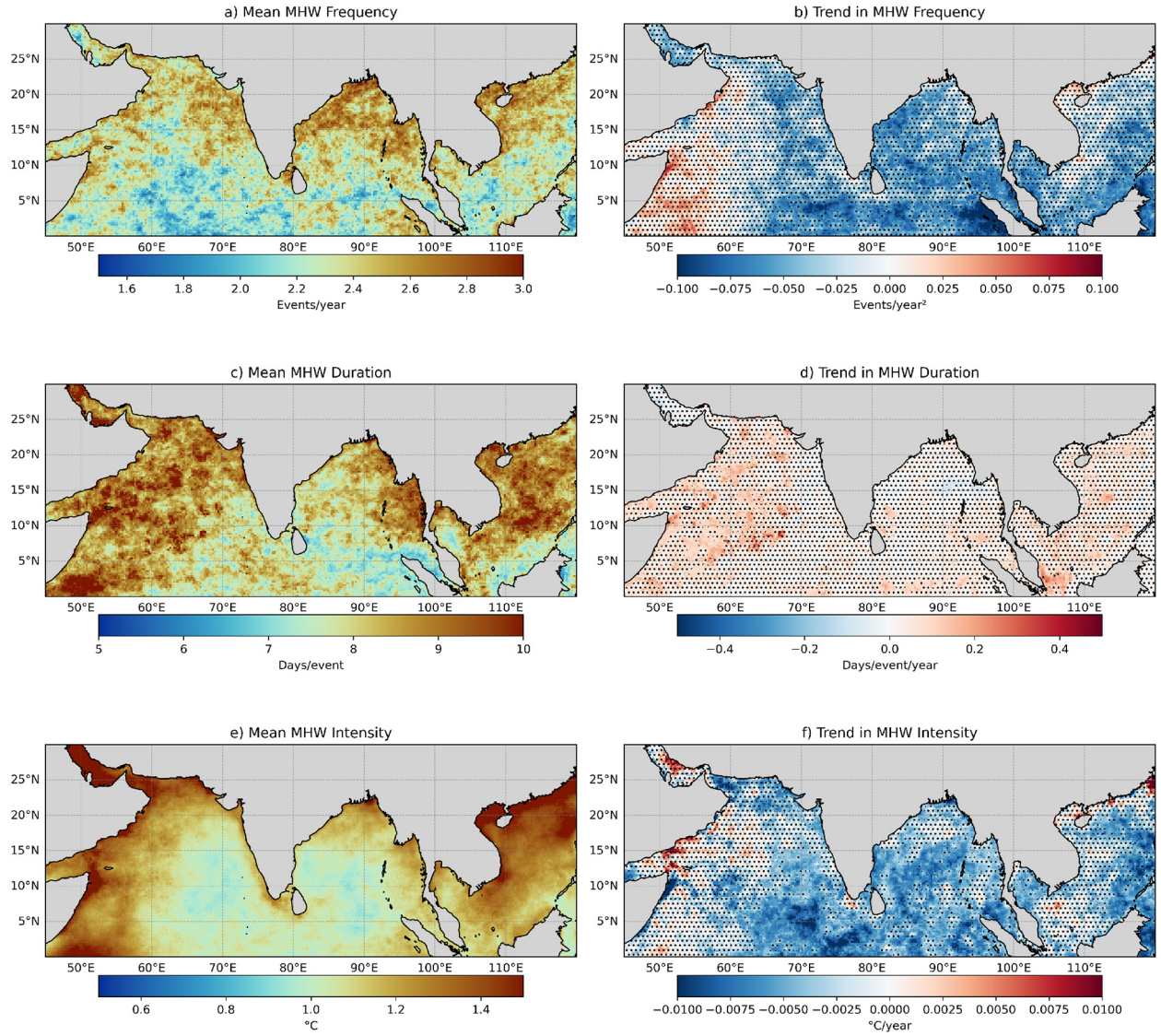

FIGURE 1
Spatial maps of **(a)** mean annual frequency of MHW events (events/year), **(b)** linear trend in MHW frequency (events/year^2), **(c)** mean duration of MHW events (days/event), **(d)** trend in MHW duration (days/event/year), **(e)** mean intensity of MHW events (°C), and **(f)** trend in MHW intensity (°C/year) over the period 1982–2024. Hatching indicates regions where trends are not statistically significant ($p > 0.05$) based on a two-tailed linear regression test.

of its widely used observational record (Reynolds et al., 2002). Our analysis covers the period 1982–2024, during which both ERA5 and OISST provide consistent and reliable data. Notably, similar results are found when using OISST, indicating that our conclusions are not sensitive to the choice of SST dataset (see Supplementary Figures S14–S16).

2.2 Marine heat waves classification

The MHWs are typically defined as periods when daily SST anomalies exceed the seasonally varying 90th percentile threshold for five or more consecutive days (Hobday et al., 2016). This threshold is usually computed using a fixed baseline climatology. However, recent studies have highlighted a key limitation of this approach. As global SSTs rise, the frequency of MHWs defined relative to a fixed baseline can increase artificially, causing the "unusual" to become the "new normal" (Jacox, 2019; Rosselló et al., 2023; Amaya et al., 2023; Capotondi et al., 2024). To address this, it has been proposed that the definition of MHWs should depend on the intended impact being assessed. For instance, when studying biological impacts such as the adaptability of marine organisms, a fixed baseline may be appropriate, as it captures absolute thermal stress relative to a historical normal. In contrast, for assessing climate impacts, particularly those related to atmospheric feedbacks and precipitation, a moving baseline or detrended SST anomalies should be used to better isolate episodic extreme events from long-term warming. Some recent studies have further recommended reserving the term "marine heatwave" for events defined using a moving climatology (Amaya et al., 2023).

In this study, we define MHWs using detrended SST anomalies. An event is identified as an MHW when the detrended SST anomaly

exceeds the seasonally varying 90th percentile for at least five consecutive days. The percentile threshold and the anomalies are calculated using the full 1982–2024 period. A seasonal climatology is first constructed using an 11-day centered moving window to capture day-to-day variability. Then this climatology is smoothed using a 31-day binomial filter to ensure temporal coherence and reduce high-frequency noise (Hobday et al., 2016). The mean and linear trends of key MHW metrics, including the frequency, duration, and mean intensity, computed using the detrended SST anomalies, are shown in Figure 1. The frequency of MHW events is higher in the Bay of Bengal compared to the Arabian Sea, whereas the MHWs in the Arabian Sea tend to last longer and show higher mean intensity. Although we do not observe widespread statistically significant trends in these metrics based on detrended SSTs, unlike studies using a fixed baseline that report significant increases (Saranya et al., 2022; Chatterjee et al., 2022; Gao et al., 2022; Kumar et al., 2023), but some regional patterns emerge. In particular, MHW duration shows a significant increasing trend across some portion of the Arabian Sea, while the Bay of Bengal exhibits a significant decrease in MHW intensity.

To understand and quantify the importance of detrending SSTs in the identification of MHWs, we present the following example using OISST. We focus on basin-scale MHW events, defined as those covering at least 25% of the basin and lasting for a minimum of 15 consecutive days, in both the Arabian Sea and the Bay of Bengal. Using detrended SST anomalies, we identified 20 events in the Arabian Sea and 17 in the Bay of Bengal, compared to 17 and 24 events, respectively, using raw (non-detrended) SSTs. Notably, before 2010, 12 MHW events were detected in the Arabian Sea and 9 in the Bay of Bengal using detrended anomalies, whereas only 1 and 2 events, respectively, were identified using non-detrended SSTs. In contrast, after 2010, 8 events were identified in each basin using detrended data, while 16 events in the Arabian Sea and 22 in the Bay of Bengal were found using raw SSTs. This clearly illustrates that failing to remove long-term warming trends can lead to an overestimation of recent MHW frequency. For instance, in 2023 alone, 202 MHW days were identified in the Arabian Sea and 93 in the Bay of Bengal using raw SSTs, compared to only 55 and 0 days, respectively, using detrended anomalies. These results underscore the necessity of detrending to accurately characterize episodic heat extremes rather than long-term background warming.

2.3 Climate indices

To assess the influence of large-scale modes of natural climate variability, such as the ENSO and the IOD, we utilize the Niño-3.4 index (for ENSO) and the Dipole Mode Index (DMI, for the IOD). The Niño-3.4 index is defined as the area-averaged SST anomalies over the Niño-3.4 region (5°N–5°S, 170°–120°W), relative to a 1981–2010 climatology. The DMI represents the anomalous SST gradient between the western equatorial Indian Ocean (50°–70°E, 10°S–10°N) and the southeastern equatorial Indian Ocean (90°–110°E, 10°S–0°). Both indices are obtained from the NOAA Physical Sciences Laboratory (NOAA PSL), where they are computed using the HadISST1.1 dataset (Rayner et al., 2003).

3 Variability of marine heatwaves in the North Indian Ocean

To understand the variability of MHWs in the North Indian Ocean, we performed an Empirical Orthogonal Function (EOF) analysis on daily MHW intensity (SST during MHW), derived from detrended SST anomalies during MHW events. Two dominant modes were identified, and their spatial patterns along with the corresponding normalized principal components (PC) are shown in Figure 2. The first mode, which explains approximately 22% of the total variance, exhibits a basin-wide pattern characterized by high MHW intensity across the central and southwest Arabian Sea, highlighting this region as a hotspot of strong MHW events. The second mode displays a dipole-like structure between the Arabian Sea (except north) and the Bay of Bengal regions, showing suppressed MHW activity (blue shading) in one basin, coinciding with enhanced activity in the other, and vice versa. Unlike Mode 1, the normalized PC time series of Mode 2 displays a more symmetric distribution between positive and negative phases (relative to Mode 1), suggesting alternating dominance of MHWs between the two basins, although positive events occur somewhat more frequently than negative ones. This mode explains approximately 8% of the total variance.

Previous studies have shown that large-scale natural climate variability modes, such as the ENSO and the IOD, can strongly influence the frequency, intensity, and duration of MHWs (see Capotondi et al., 2024; for a recent review; Gao et al., 2022; Chatterjee et al., 2022; Swetha et al., 2025; Sandaruwan et al., 2023). To explore these relationships, we computed monthly lead-lag correlations between the PCs of the two dominant modes and the Niño 3.4 index (representing ENSO) and the Dipole Mode Index (DMI, representing the IOD). The results are shown in Figure 3. The highest correlation (0.5) is observed between PC1 and Niño 3.4 when Niño 3.4 leads by approximately 5 months. This suggests that the basin-wide MHW pattern represented by PC1 may be linked to the mature phase of ENSO. This relationship is consistent with the Indian Ocean Basin Mode (IOBM), where ENSO induces basin-wide warming in the Indian Ocean with a few months lag (Klein et al., 1999; Xie et al., 2009; Guo et al., 2017). The strong lagged correlation between PC1 and Niño 3.4, along with the similarity to the IOBM, suggests that basin-wide MHWs in the North Indian Ocean can be largely modulated by ENSO via the Indian Ocean Basin Mode. This is consistent with Chatterjee et al. (2022) who showed that 70–80% of MHWs in the Arabian Sea are influenced by the Indian Ocean Basin mode through the decaying phase of ENSO. PC1 also shows a weaker but noticeable correlation with DMI (0.3) when DMI leads by about 2 months. However, since the correlation between Niño 3.4 and DMI also peaks at this lag, the PC1-DMI correlation may simply reflect the influence of ENSO on the IOD rather than an independent effect of the IOD itself (see Supplementary Figure S1 for lead–lag partial correlation between the DMI and the PC time series after statistically removing the influence of Niño 3.4). Similarly, the PC2 correlation with Niño 3.4 is relatively less compared to PC1. The maximum correlation (−0.3) occurs when PC2 leads Niño 3.4 by about 2 months, suggesting a link between PC2 and La-Niña. These findings imply that large-scale climate modes, particularly ENSO,

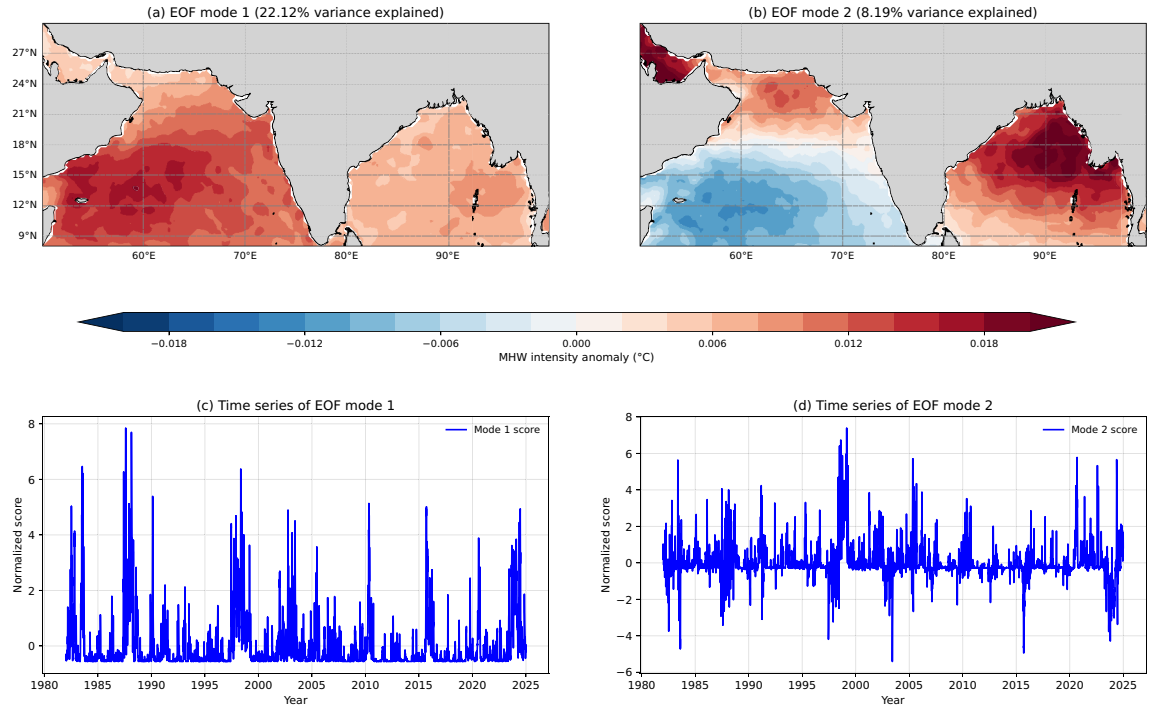

FIGURE 2
Empirical Orthogonal Function (EOF) analysis of the MHW intensity in the North Indian Ocean using ERA5 SST (based on daily data for all months, not limited to JJAS). **(a)** Spatial pattern of the leading mode (Mode 1). **(b)** Spatial pattern of the second mode (Mode 2). **(c)** Normalized principal component time series corresponding to Mode 1. **(d)** Normalized principal component time series corresponding to Mode 2.

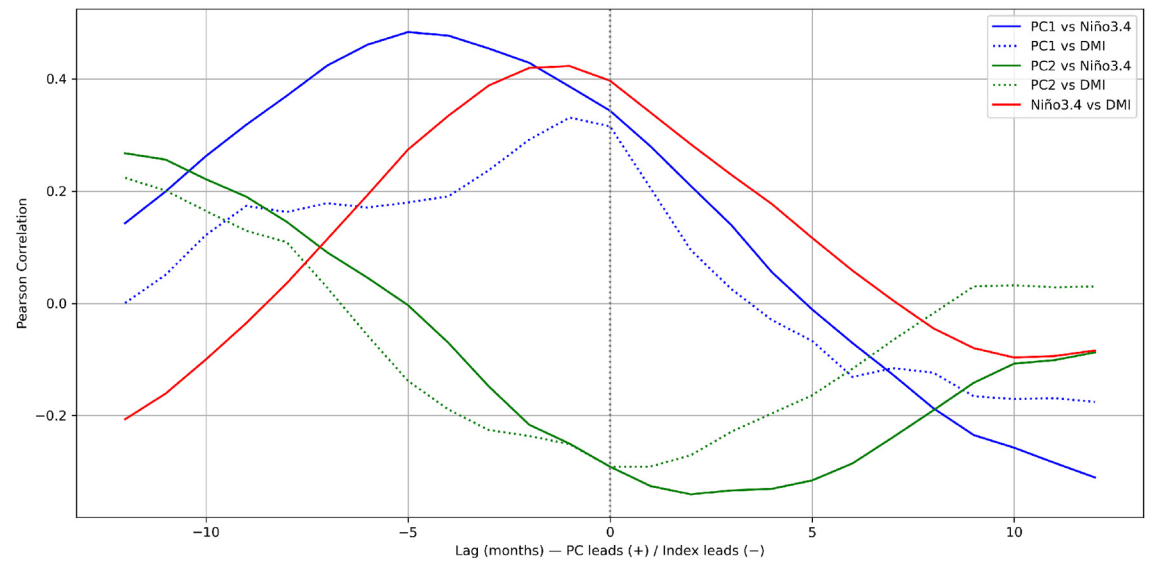

FIGURE 3
Lead-lag correlations between the PCs (converted to monthly) and climate indices. Blue and green lines represent correlations involving PC1 and PC2, respectively. Solid lines denote correlations with Niño 3.4, while dashed lines denote correlations with the DMI. The red line shows the correlation between Niño 3.4 and DMI. Negative lags indicate the climate index leads the PC, while positive lags indicate the PC leads the index.

might play a crucial role in driving the variability of MHWs in the North Indian Ocean.

To further investigate the ENSO–MHW relationship, Figure 4 shows the frequency of MHWs during El Niño, neutral, and La Niña conditions. During El Niño, MHW frequency is enhanced over the central and southern Arabian Sea, with comparatively lower frequencies over the Bay of Bengal, closely resembling the spatial structure of the PC1 and PC2- modes. In contrast, MHW frequency during La Niña is generally weaker than during El Niño but exhibits pronounced maxima over the Bay of Bengal and the

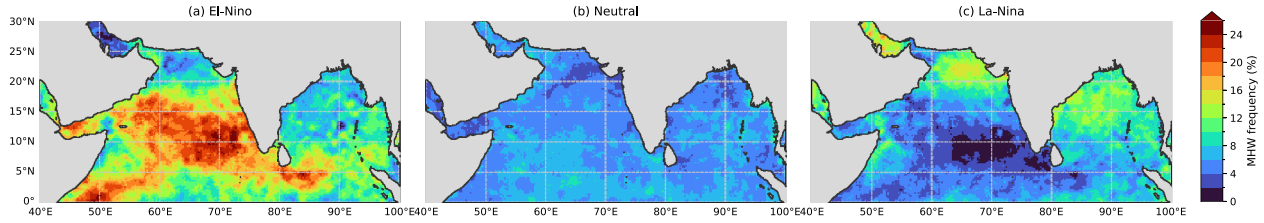

FIGURE 4
MHW frequency (%) during different ENSO phases over the Indian Ocean. **(a–c)** Show the spatial distribution of MHW frequency during El Niño, Neutral, and La Niña conditions, respectively. The color scale indicates the percentage of time steps classified as marine heatwaves within each ENSO phase.

northern Arabian Sea, consistent with the positive phase of the PC2 mode. These spatial correspondences provide further support for our inference that PC1 and PC2- events usually occur during El Niño years, whereas positive PC2 events are more prevalent during La Niña years. The physical drivers underlying each mode are examined in greater detail in the following sections.

4 The drivers of marine heatwaves modes in the North Indian Ocean

To analyze the drivers of the two dominant modes of MHW variability in the North Indian Ocean, we identified extreme events based on the daily normalized MHW-intensity based PC time series (Figures 2c, d). Events were selected when the PC exceeded the seasonally varying 90th percentile (or was below the 10th percentile for the negative phase of Mode 2) for at least five consecutive days, consistent with the definition of MHWs. Our analysis is restricted to events occurring during the South Asian Monsoon season (June-September), aligning with our objective of assessing their influence on South Asian monsoon rainfall.

The leading mode of MHWs (PC1) in the North Indian Ocean corresponds to a basin-wide pattern, with MHWs covering the entire region and particularly high intensity in the Arabian Sea (Figure 2a). We identified 16 distinct events in which the PC1 time series exceeded the seasonally varying 90th percentile for at least five consecutive days. The start dates, end dates, and durations of these events are provided in Supplementary Table S1. These PC1-mode MHW events lasted between 5 and 59 days, with a median duration of 10 days and a mean duration of approximately 19 days. Interestingly, the latest three events show a duration above 20 days. Notably, 10 events out of 16 occurred during El Niño or within 5 months after El-Nino. Regression of the PC1 time series onto SST (Supplementary Figure S2a) reveals an El Niño-like SST pattern, further supporting the association between this MHW mode and El Niño conditions.

In contrast to the basin-wide structure of Mode 1, the positive phase of Mode 2 (PC2+) displays an eastwest dipole, with MHWs focused in the Bay of Bengal and an absence of MHWs in the central and southern Arabian Sea (Figure 2b). We identify 34 PC2+ events (Supplementary Table S2), most commonly during the El Niño to La Niña transition phase, with durations ranging from 5 to 35 days (mean of 12 days and median of 10 days). The negative phase of Mode 2 (PC2−) reverses the eastwest dipole, with MHW activity concentrated in the central and southern Arabian Sea and absent in the Bay of Bengal. A total of 22 such events were identified based on the PC2 time series falling below the seasonally varying 10th percentile for at least five consecutive days (Supplementary Table S3). Out of these 22 events, 8 occur during the early phase of El Niño, suggesting a possible but weaker influence of El Niño on PC2− compared to PC1, which is more strongly associated with the mature phase of El Niño.

4.1 SST and precipitation during marine heatwaves

The composite anomalies of detrended SST and precipitation overlaid with 10-meter winds during the selected extreme events for different EOF modes are shown in Figure 5. As expected from the PC1 spatial pattern, SST anomalies are strongly positive across the North Indian Ocean, including the Arabian Sea and the Bay of Bengal. The strongest warming is observed in the Arabian Sea (Figure 5a). The corresponding precipitation and 10-meter wind anomalies indicate weakening of monsoon winds (anomalous Northerly winds or weakened Southerly winds) and enhanced rainfall over the eastern Arabian Sea, southern Bay of Bengal and parts of southern India, while central and northeastern India and north of the Bay of Bengal exhibit suppressed precipitation (Figure 5d). Although the SST anomalies somewhat resemble those typically observed during a positive IOD event, the associated wind patterns deviate from the canonical IOD structure, which is characterized by strengthened cross-equatorial monsoon winds (Prajeesh et al., 2021).

The composite SST anomalies during PC2+ events show intense warming over the Bay of Bengal and parts of the northern Arabian Sea, while southern Arabian Sea SST anomalies remain neutral or slightly negative (Figure 5b). This warming is accompanied by cyclonic wind anomalies over the southeastern Arabian Sea and enhanced rainfall over southern India and the eastern Arabian Sea (Figure 5e). This is in agreement with Saranya et al. (2022), which shows that the MHW in the Bay of Bengal is associated with enhanced rainfall over southwest India. Compared to PC1, the rainfall anomalies are more intense but spatially concentrated, especially over the southern part of India. The negative of this mode is characterized by pronounced SST anomalies in the western Indian Ocean (Figure 5c), weak winds over the region, and widespread dry anomalies across India (Figure 5f). Unlike the previous two modes, this phase is associated with suppressed monsoon activity across much of the

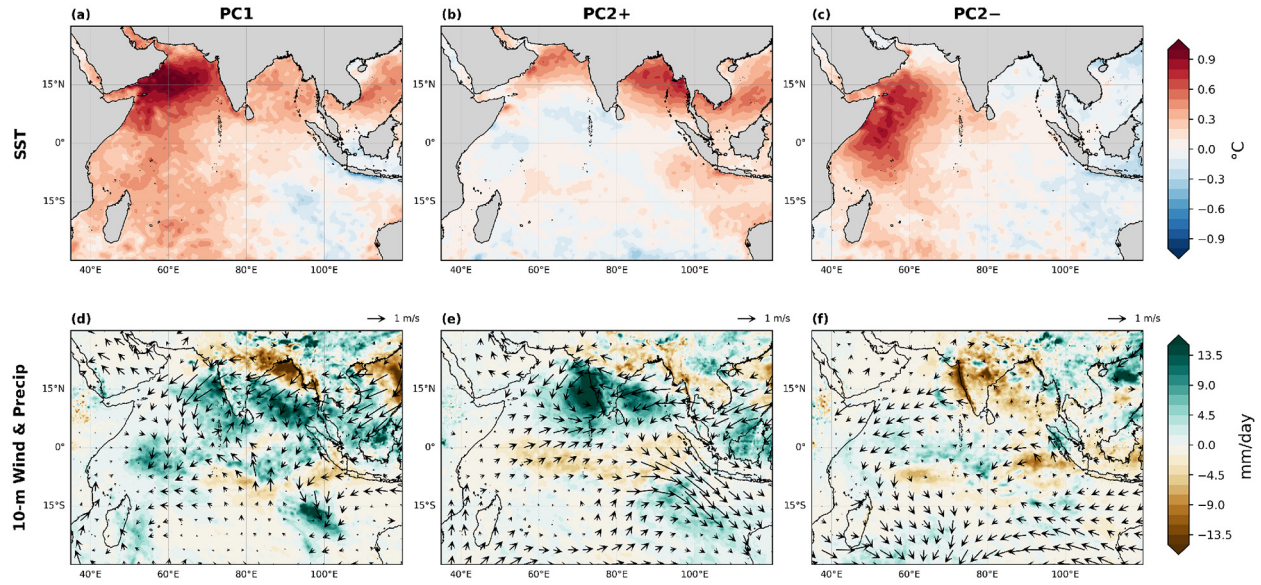

FIGURE 5
Composite anomalies of SST (top row; °C), precipitation (bottom row; shading; mm day^{-1}), and 10 m wind vectors (arrows; m s^{-1}) during MHW events associated with **(a, d)** PC1, **(b, e)** PC2+, and **(c, f)** PC2− phases.

Indian Subcontinent, likely due to weakened low-level monsoon circulation and the absence of moisture‘convergence.

4.2 Atmospheric conditions before marine heatwaves

To understand the mechanisms driving these MHW events, we performed a composite analysis of atmospheric conditions during the five days prior to each MHW event for the three selected EOF modes (Figure 6). The variables include MSLP, surface wind, surface latent heat flux (positive downward), shortwave radiation flux (positive downward), and precipitation. Sensible heat flux and longwave radiation contributions to PC1 and PC2 (see composite maps in Supplementary Figure S3), are much smaller (by an order of magnitude) as compared with both shortwave radiation and latent heat flux contributions.

For the PC1 mode, a strong positive anomalous MSLP is observed to the north of the Arabian Sea, Indian subcontinent, Bay of Bengal, and northwest Pacific, while a corresponding negative anomaly appears in the southern Indian Ocean (Figure 6a). This pattern is detrimental to the summer monsoon flow, which is driven by a pressure gradient: high pressure over the Indian Ocean and low pressure over the Indian subcontinent. As a result, these anomalies weaken the meridional pressure gradient and reduce the strength of southwesterly monsoon winds, as evident in the weakened cross-equatorial wind flow (Figure 6d). The weakening of surface winds reduces evaporation, which is reflected in the decreased upward latent heat flux (positive downwards) from the ocean to the atmosphere (Figure 6g). Lower evaporation rates could lead to fewer clouds (Supplementary Figure S4), allowing more incoming shortwave radiation to reach the ocean surface (Figure 6j). This radiative forcing, combined with reduced air-sea turbulent heat fluxes to the atmosphere, in turn driven by reduced winds, further enhances upper-ocean warming. The weaker winds can also reduce the wind-driven upper ocean mixing and have the potential to contribute to the ocean warming. The precipitation pattern shows dry conditions over western and central India and north of the Bay of Bengal, and wet conditions in the eastern equatorial Indian Ocean.

The atmospheric precursors of PC2+ mode MHWs also feature a reversal in the monsoon pressure gradient but with more localized intensity over the Bay of Bengal. Strong positive sea-level pressure anomalies are centered over the northern Bay of Bengal and the northwest Pacific, while a deep low persists over the southeastern Indian Ocean (Figure 6b). Compared to PC1, the gradient is sharper in the eastern basin, leading to more pronounced weakening of surface winds over the Bay of Bengal (Figure 6e). This suppresses evaporation and upward latent heat flux, inducing reduced cloud cover and, in turn, increased solar radiation to enhance warming of the upper ocean (Figures 6h, k). The spatial confinement of this air-sea feedback (particularly the latent and shortwave flux) over the Bay of Bengal explains the eastward focus of MHWs in this mode. The precipitation pattern shows dry conditions north of the Bay of Bengal and wet conditions in the eastern equatorial Indian Ocean (Figure 6n).

For the PC2- mode, the composite atmospheric anomalies reveal a distinct pressure structure. Elevated MSLP anomalies appear entirely over the north Indian Ocean, with high values over the eastern Arabian Sea near the Gulf region, with a corresponding low in the southwestern Indian Ocean (Figure 6c). This configuration again opposes the typical monsoon pressure gradient, weakening the cross-equatorial winds, this time primarily over the western basin (Figure 6f). Reduced wind speeds lead to suppressed evaporation and latent heat loss (Figure 6i), consistent with sea surface warming.

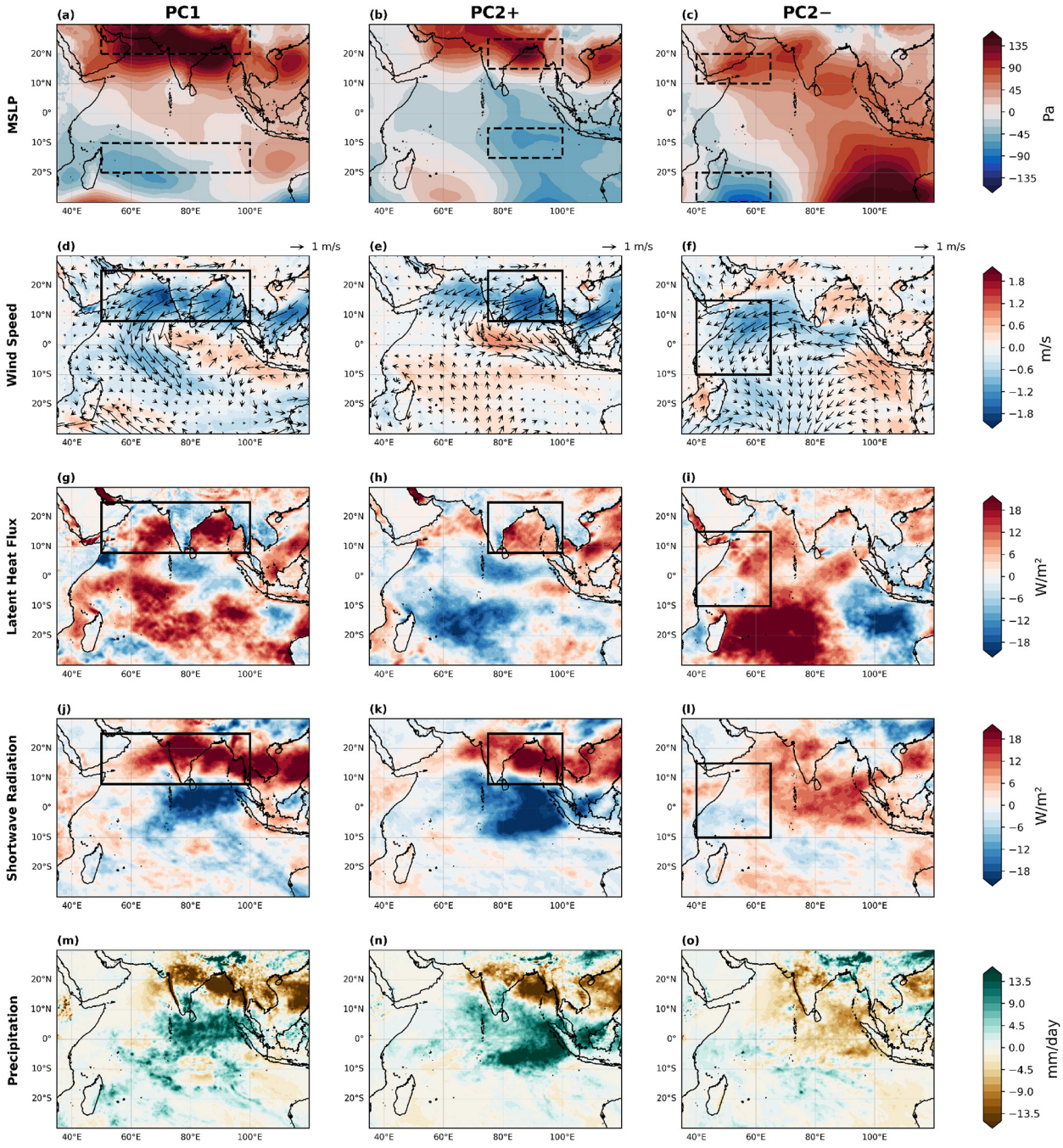

FIGURE 6
Composite anomalies averaged over the 5 days preceding MHW onset for different modes: PC1 (left column), PC2+ (middle column), and PC2− (right column). Panels show **(a–c)** mean sea level pressure anomalies (Pa), **(d–f)** 10 m wind speed anomalies (shading; m s^{-1}) with wind vector anomalies (arrows), **(g–i)** latent heat flux anomalies (W m^{-2}; positive downward), **(j–l)** shortwave radiation anomalies (W m^{-2}; positive downward), and **(m–o)** precipitation anomalies (mm day^{-1}). Boxes indicate the domains used to compute spatial means for the time series analysis (see Figure 7).

However, unlike the other modes, there is no substantial enhancement in shortwave radiation in this region, suggesting that MHW formation here is primarily driven by suppressed turbulent cooling rather than radiative forcing (Figure 6l). Furthermore, the weakening of nearshore winds along the Somali coast in the western Indian Ocean can suppress upwelling, thereby having the potential to reduce upwelling-induced cooling and contribute to elevated SSTs in the region. The precipitation anomaly shows dry conditions throughout India (Figure 6o).

The composite anomaly patterns exhibit striking similarities to those associated with the Monsoon Intra-Seasonal Oscillation (MISO), particularly for the positive phases of PC1 and PC2, suggesting a potential role of MISO in modulating MHWs. Therefore, the influence of MISO on MHW variability is examined in a subsequent section.

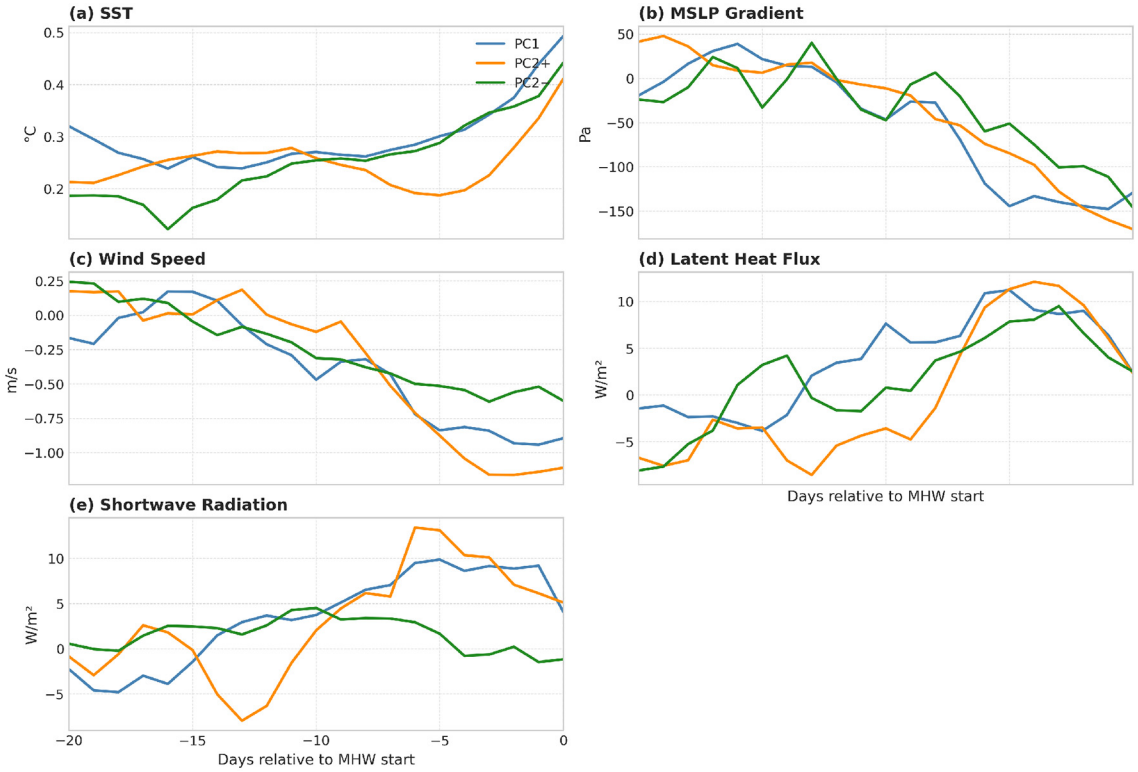

FIGURE 7
Time series of composite anomalies associated with MHW onset in the North Indian Ocean for PC1 (blue), PC2+ (orange), and PC2- (green) modes. Spatial means were computed over the boxed regions shown in Figure 6: PC1 over 8°–25°N, 50°–100°E; PC2-positive over 8°–25°N, 75°–100°E; and PC2-negative over 10°S–15°N, 40°–65°E. For **(b)**, the mean sea level pressure gradient was calculated for each mode as the meridional difference between the southern and northern bands (dashed boxes in Figure 6): PC1: 10°S–20°S and 20°–30°N (averaged over 50°–100°E), PC2-positive: 5°S–15°S and 15°–25°N (averaged over 75°–100°E), and PC2-negative: 20°S–30°S and 10°–20°N (averaged over 40°–65°E). **(a)** Sea surface temperature anomaly (°C). **(b)** Mean sea level pressure gradient anomaly (Pa). **(c)** 10-meter wind speed anomaly (m/s). **(d)** Latent heat flux anomaly (W/m; positive downward). **(e)** Shortwave radiation anomaly (W/m; positive downward). Day 0 corresponds to the MHW onset date.

4.3 Evolution of atmospheric drivers and SST leading to marine heatwaves

The evolution of SST and atmospheric variables across the MHW hotspot regions relative to MHW onset is shown in Figure 7. For the PC1 mode, SST anomalies begin to emerge roughly 8 days prior to the MHW onset (Figure 7a), following an early weakening of the meridional MSLP gradient (calculated as the meridional difference between 30°S–20°S and 10°N–20°N, averaged along the same longitude), starting up to 16 days before onset and becoming pronounced around 8 days before the onset (Figure 7b). Wind speeds decline in parallel, further reducing surface evaporation (Figure 7c). Latent heat flux anomalies peak 6 days prior (Figure 7d), consistent with diminished turbulent cooling. Meanwhile, shortwave radiation increases steadily, peaking before onset and staying elevated afterward (Figure 7e). The correlation analysis between key variables supports this hypothesis. A strong positive correlation is observed between MSLP and wind speed ($r = 0.9$ at lag 0), while wind speed and latent heat flux exhibit a strong negative correlation ($r = -0.8$ at lag 0). Additionally, latent heat flux is strongly correlated with shortwave radiation ($r = 0.9$). Shortwave radiation and SST show a significant positive correlation ($r = 0.8$) with a lag of 5 days. Moreover, SST demonstrates similarly high correlations with other variables, including MSLP, wind speed, and latent heat flux, all with a lag of 5 days, highlighting their potential roles in modulating SST variability.

For the Bay of Bengal (8°–25°N, 75°–100°E), PC2+ MHW events are preceded by a distinct atmospheric evolution (Figure 7). SST anomalies begin to develop just 4 days before onset (Figure 7a), while the MSLP gradient (calculated as the meridional difference between 5°S–15°S and 15°N–25°N, averaged along the same longitude) weakens over a longer window, starting 20 days prior to the onset, with a marked decline beginning 9 days before (Figure 7b). Wind speed anomalies sharply drop in this period (Figure 7c), triggering suppressed latent heat loss that peaks around 4 days before onset (Figure 7d). Shortwave radiation intensifies steadily (Figure 7e), with a magnitude similar to that of the latent heat flux anomaly. While the sequence mirrors PC1, the atmospheric anomalies are stronger and more localized over the Bay of Bengal, reinforcing the regional intensity and structure of PC2-positive events.

The evolution of drivers for PC2- events focused on the western Indian Ocean (10°S–15°N, 40°–65°E), shows subtle yet important distinctions (Figure 7). SST anomalies begin building as early as 16 days prior to MHW onset (Figure 7a), with weakening of the MSLP gradient observed from around 2 weeks prior to the onset (Figure 7b). Wind speeds begin a slower, more gradual decline from 18 days before onset (Figure 7c), leading to reduced evaporation

and reduced latent heat fluxes from ocean to atmosphere, peaking 4 days before onset (Figure 7d). Shortwave radiation anomalies rise but remain relatively moderate and even dip a few days before the onset (Figure 7e). Unlike the other two modes, turbulent heat contributions are higher compared to the radiative heating, suggesting a dominance of the latent heat component (and plausibly reduced upwelling, as discussed in the previous section) in driving this mode.

5 Monsoon intraseasonal oscillation and marine heatwaves

The Indian summer monsoon exhibits pronounced intraseasonal variability from May to October, commonly referred to as the Monsoon Intraseasonal Oscillation (MISO) (Goswami and Mohan, 2001; Rajeevan et al., 2010). MISO is characterized by alternating active (wet) and break (dry) phases, each typically persisting for several days. Numerous studies have demonstrated a two-way interaction between MISO-related precipitation anomalies and SST variability, whereby atmospheric forcing associated with MISO influences SST, and SST anomalies, in turn, modulate MISO rainfall (Kemball-Cook and Wang, 2001; Vecchi and Harrison, 2002; Fu et al., 2003, 2007; Roxy and Tanimoto, 2007; Krishnamurthy and Kirtman, 2009; Zhang L. et al., 2018). For instance, Vecchi and Harrison (2002) showed that SST cooling in the northern Bay of Bengal precedes monsoon break phases by approximately 1 week, while Roxy and Tanimoto (2007) demonstrated that positive SST anomalies over the Arabian Sea lead enhanced precipitation during the active phase of MISO. These findings suggest that MISO-related air-sea interactions may also play an important role in the development and modulation of MHWs, an aspect that is examined in this section.

MISO phases are derived using Extended Empirical Orthogonal Function analysis (Suhas et al., 2012). Composite anomalies of precipitation, MSLP, near-surface winds, and latent heat flux during the eight MISO phases, computed using the ERA5 rainfall data (see Supplementary Figures S5–S8), align with those shown by Suhas et al. (2012) using IMD data. For example, during MISO Phase 1, enhanced convection is centered near the equator, which then migrates northward over subsequent phases. Similarly, an anomalous high-pressure center is seen over the Indian subcontinent during the initial four phases, transitioning to low pressure in the later phases. Interestingly, some of these MISO composite patterns resemble the pre-MHW conditions seen in different EOF modes of MHWs. For example, the precipitation anomaly patterns during PC1 and PC2+ (see Figures 5) are similar to those during MISO Phases 4 and 5, where enhanced convection is concentrated over the southern India and Bay of Bengal, with suppressed rainfall over central India and the northern Bay of Bengal. Likewise, the MSLP and precipitation anomalies observed 5 days prior to MHW onset (Figure 6) resemble those seen during MISO Phase 3 (Supplementary Figures S5, S6).

To examine the interaction between MISO and MHWs more systematically, we further analyzed the daily percentage occurrence of each MISO phase from 10 days before to 10 days after MHW onset for events in each EOF mode (Supplementary Figure S9). In PC1, we observe a sequential transition from MISO Phase 1 (centered around day −10) to Phase 3 (around day 0), followed by a scattered distribution of Phases 4 and 5 after the onset. This suggests a potential link between the early MISO phases and the buildup toward MHW events in PC1. The progression is more coherent in PC2+, where a clear temporal propagation from Phase 1 through Phase 5 is visible from day −10 to day 10. Particularly, Phase 2 and Phase 3 dominate in the days immediately leading up to MHW onset (with occurrence frequencies exceeding 30%), followed by the transition to Phases 4 and 5 in the post-onset days. This indicates that MHWs of PC2+ often arise during initial MISO events. In contrast, PC2− events show a markedly different evolution, with MISO Phases 6–8 dominating around the time of MHW onset (days −3 to +1). This suggests that PC2− MHWs tend to occur during the later stages of the MISO cycle and exhibit a weaker dependence on MISO phase evolution compared to PC1 and PC2+.

We further examined the frequency of MHW occurrence during each MISO phase (Figure 8). MHW frequency over the North Indian Ocean peaks during MISO Phase 4 and remains elevated during Phase 5. Taken together with the onset-phase analysis, this indicates that MHWs are most often initiated during MISO Phases 3–4, when surface winds are weak and evaporative cooling is reduced (Supplementary Figures S7, S8), creating favorable conditions for ocean surface warming. The persistence of elevated MHW frequency into Phase 5, despite a recovery of winds and latent heat loss, highlights the role of upper-ocean heat storage and memory, allowing MHWs initiated earlier to persist beyond the phase of weakest surface forcing. Overall, these results support a modulation of North Indian Ocean MHW variability by MISO-related surface conditions, consistent with previous studies showing an influence of intraseasonal variability on SST (Kemball-Cook and Wang, 2001; Vecchi and Harrison, 2002; Fu et al., 2003, 2007; Roxy and Tanimoto, 2007; Zhang L. et al., 2018).

In addition to intraseasonal variability, interannual variability associated with ENSO can further modulate MHW occurrence (Section 3). To explore ENSO-MISO-MHW interactions, we computed MHW frequency separately for El Niño and La Niña conditions during MISO Phases 4–5 (Figure 9). Consistent with Figures 4, 8, La Niña conditions are associated with higher MHW frequency over the Bay of Bengal relative to the Arabian Sea during these phases, resembling the PC2+ pattern, whereas El Niño conditions favor enhanced MHW frequency over the Arabian Sea compared to the Bay of Bengal, resembling the PC1 pattern. During El Niño years, basin-wide SST anomalies are positive across much of the North Indian Ocean, with pronounced warming over the Arabian Sea (Supplementary Figure S10), which can precondition the region for MHW development during suppressed/break-like MISO conditions (e.g., Phase 3) (Yang et al., 2007; Xie et al., 2009; Abish et al., 2017). Conversely, during La Niña years, the background state differs (Supplementary Figure S11), and the

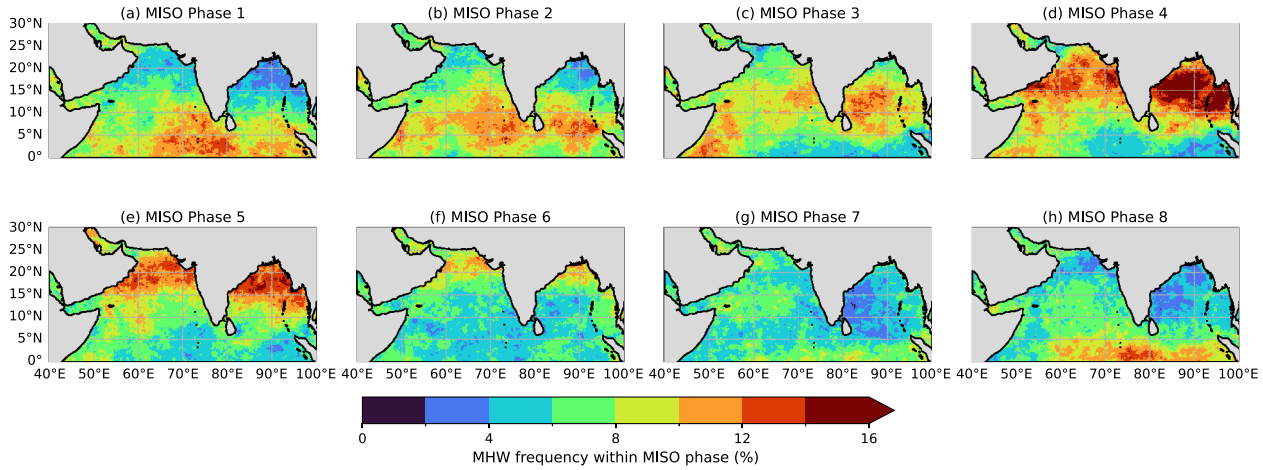

FIGURE 8
Spatial distribution of MHW frequency (%) during different phases of MISO. **(a–h)** Correspond to MISO phases 1–8, respectively. MHW frequency is defined as the percentage of time steps classified as MHWS within each MISO phase.

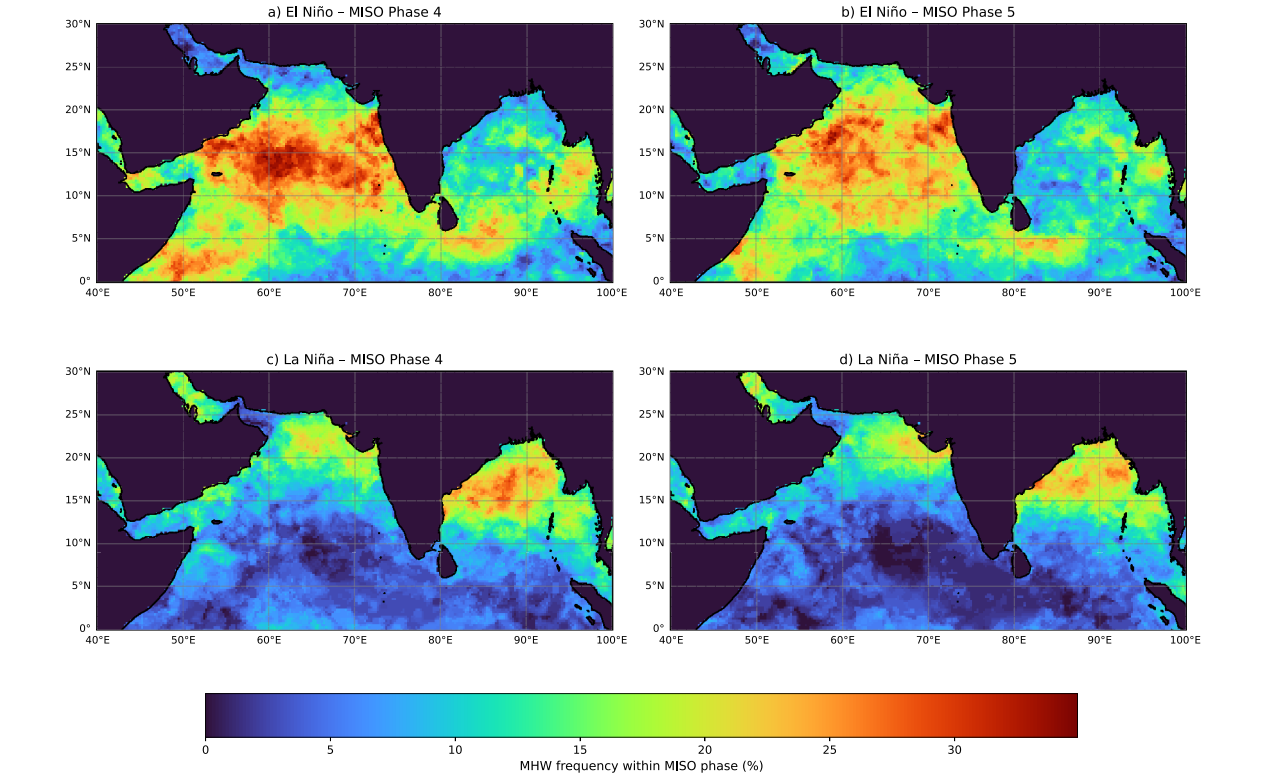

FIGURE 9
Spatial distribution of marine heatwave (MHW) frequency (%) during MISO Phases 4 and 5 under different ENSO conditions: **(a)** El Niño during MISO Phase 4, **(b)** El Niño during MISO Phase 5, **(c)** La Niña during MISO Phase 4, and **(d)** La Niña during MISO Phase 5.

associated circulation anomalies can favor reduced winds and weaker evaporative cooling over the Bay of Bengal, thereby increasing the likelihood of localized MHW development (Krishnamurthy and Kirtman, 2009). Together, these results suggest that intraseasonal (MISO) and interannual (ENSO) variability can interact to shape the spatial distribution of North Indian Ocean MHW occurrence.

6 The post-marine heatwaves impact on the summer monsoon rainfall

The composite of key atmospheric variables averaged over 5 days following the MHW end dates (Figure 10), reveals contrasting patterns compared to those observed prior to the MHW events, with enhanced rainfall over the Indian Subcontinent.

For the PC1 mode, negative pressure anomalies are evident over the North Indian Ocean, particularly over the Arabian Sea (Figure 10a). High SSTs during MHWs can slowly heat the air immediately above the ocean surface, increasing air temperature. This warmer air becomes less dense and rises, leading to divergence at higher altitudes. By mass continuity, this upward motion induces a decrease in surface pressure. The time lag between warm air rising and upper-level divergence is important to account for when explaining the impact of MHWs on atmospheric variables a few days later. The regression analysis between SST and MSLP during the MHW days for the three different modes shows negative values across most of the North Indian Ocean, indicating that SST and MSLP are inversely related (Supplementary Figure S12). This reduction in anomalous pressure helps strengthen the climatological monsoon pressure gradient, characterized by low pressure over the Indian subcontinent and high pressure over the southern Indian Ocean, which, in turn, enhances the monsoon circulation (Figure 10d). These strengthened winds promote increased evaporation over the ocean, as reflected in the negative latent heat flux anomalies (Figure 10g), indicating more heat being transferred from the ocean (which was stored during the MHW event) to the atmosphere. This enhanced evaporation also supports greater cloud formation, which in turn limits the amount of incoming solar radiation reaching the ocean surface (Figure 10). As a result, the ocean loses heat both through latent heat flux and reduced radiative input, helping to terminate the MHW event. These post-MHW atmospheric adjustments are accompanied by enhanced precipitation over western and northeastern India, Bangladesh, Myanmar, and the Bay of Bengal region (Figure 10m). The increased evaporation over the Arabian Sea possibly contributes to greater moisture availability, which is subsequently transported toward western and central India, as indicated by the anomalous vertically integrated water vapor transport (IVT) vectors. Similarly, elevated evaporation over the Bay of Bengal possibly enhances moisture convergence over northeastern India, Myanmar, Bangladesh, and the Bay of Bengal, consistent with strengthened IVT directed toward these regions. This spatial pattern suggests a potential feedback mechanism, wherein MHW-induced ocean-atmosphere interactions can amplify monsoon rainfall following the decay of a basin-wide MHW event, consistent with the previous studies on MISO-SST monsoon rainfall interactions (Roxy and Tanimoto, 2007; Zhang L. et al., 2018).

Post-event atmospheric anomalies for PC2+ MHWs closely resemble the recovery seen in PC1. A negative MSLP anomaly persists over the Bay of Bengal, central India, and the Arabian Sea (Figure 10b), enhancing the meridional pressure gradient and reviving monsoon winds across both basins (Figure 10e). These stronger winds increase latent heat release (Figure 10h) and cloud formation, which acts to reduce incoming shortwave radiation (Figure 10k). The combination of turbulent and radiative heat loss contributes to the decay of warm anomalies in the Bay of Bengal, terminating the MHW phase. Following PC2+ MHW events, precipitation intensifies primarily over central India and the northern Bay of Bengal (Figure 10n). Increased evaporation from both basins enhances atmospheric moisture, which then converges over these regions, as indicated by strengthened IVT anomalies directed toward central India and the northern Bay of Bengal.

The termination phase of PC2- MHWs displays some differences. A broad negative pressure anomaly forms over central India and the Arabian Sea (Figure 10c), strengthening monsoon flow particularly in the southern Arabian Sea and across southern India (Figure 10f). However, winds remain weak over the northern Arabian Sea and north India, generating an anomalous cyclonic pattern over the subcontinent. In the southern basin, increased evaporation (Figure 10i) and diminished shortwave radiation (Figure 10l) accelerate ocean heat loss. Post-event rainfall anomalies for PC2-negative events are concentrated over southern and central India, as well as parts of the Bay of Bengal, which are the regions influenced by an anomalous cyclonic circulation (Figure 10o). Moisture buildup from enhanced evaporation in the western Indian Ocean likely fuels this rainfall response, with anomalous IVT vectors indicating moisture transport toward southern India. While the overall feedback resembles that of the other modes, the southward shift in rainfall highlights the spatial sensitivity of monsoon response to MHW positioning and termination dynamics.

Moreover, the precipitation composite anomalies, particularly for PC1 and PC2+, closely resemble the characteristic precipitation patterns during MISO Phases 6 and 7 (Supplementary Figure S5), which are typically associated with enhanced convective activity over the Indian region. In addition, our analysis reveals that approximately 33% of the total MHW events associated with PC1 and PC2+ terminate during MISO Phase 6, further highlighting a strong interaction between MISO variability and MHW evolution in the North Indian Ocean. To examine this interaction in more detail, we identified MHW events that terminate during MISO Phase 6 for PC1 and PC2+ and computed the precipitation differences during MISO Phases 6 and 7 relative to MISO cycles without any MHW activity. The resulting composites (Supplementary Figure S13) isolate the potential influence of MHW termination on MISO rainfall during a dynamically active phase of the intraseasonal monsoon. For PC1, the precipitation differences during MISO Phases 6 and 7 indicate drying over much of India, particularly over central India, accompanied by anomalous wetting over the eastern Bay of Bengal, Bangladesh, and surrounding regions. In contrast, PC2+ events are associated with anomalous wetting over Gujarat and the adjacent coastal regions of the Arabian Sea, central India, and the northern Bay of Bengal. Similar, though generally weaker and less spatially coherent, precipitation differences are obtained when conditioning on MHW presence during MISO Phases 4 and 5 (not shown), suggesting that MHWs may also influence MISO rainfall during their persistence, albeit less robustly than during their termination. Notably, while these precipitation responses share some similarities with canonical SST-MISO rainfall patterns, the MHW-conditioned composites exhibit distinct spatial structures, reflecting the role of extreme and spatially coherent ocean warming rather than background SST variability alone. Together, these results suggest that MHWs can modulate MISO rainfall, in addition to the influence of MISO variability on MHW evolution. A detailed investigation of the physical mechanisms underlying these interactions is beyond the scope of this study and is left for future work.

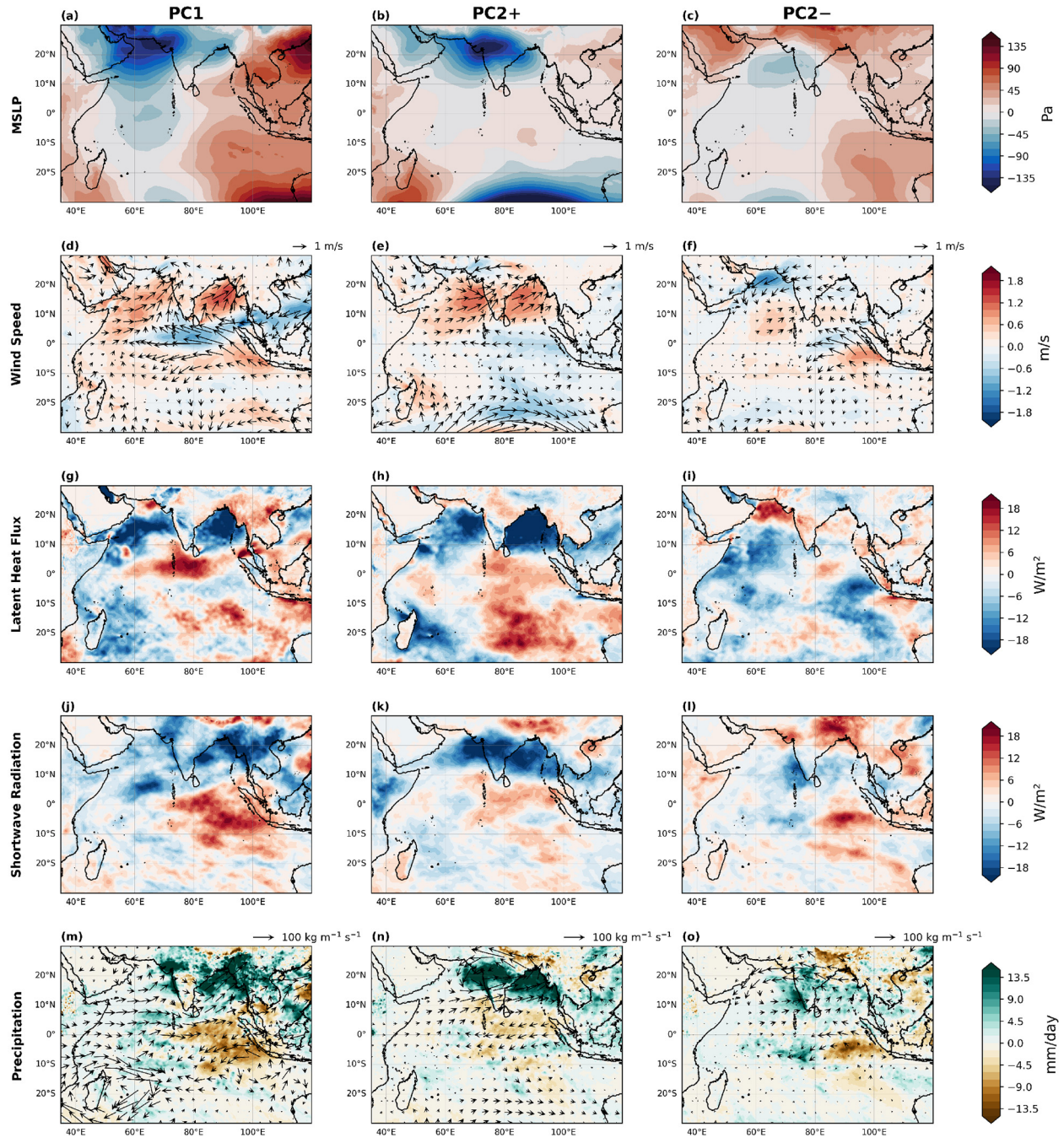

FIGURE 10
Composite anomalies averaged over the 5 days following MHW termination for different modes: PC1 (left column), PC2+ (middle column), and PC2− (right column). Panels show **(a–c)** mean sea level pressure anomalies (Pa), **(d–f)** 10 m wind speed anomalies (shading; m s^{-1}) with wind vector anomalies (arrows; m s^{-1})), **(g–i)** latent heat flux anomalies (W m^{-2}; positive downward), **(j–l)** shortwave radiation anomalies (W m^{-2}; positive downward), and **(m–o)** precipitation anomalies (shading; mm day^{-1}) with vertically integrated water vapor (IVT) flux vector anomalies (arrows; kg m^{-1} s^{-1}).

7 Summary and discussion

MHWs are typically defined as periods when daily SST anomalies exceed the seasonally varying 90th percentile threshold, calculated using a fixed climatology, for five or more consecutive days. However, recent studies have indicated that using a fixed baseline can artificially raise the observed increase in MHW frequency as global SSTs rise, effectively making the "unusual" the "new normal." To address this issue, we defined MHWs using detrended SST anomalies, thereby isolating internal variability from long-term warming, and investigated the variability, drivers, and monsoon impacts of MHWs in the North Indian Ocean.

To objectively isolate the dominant spatial structures of MHW variability, we apply an EOF analysis to MHW intensity. This approach identifies coherent, large-scale MHW patterns directly from the data, avoiding the need for arbitrary thresholds based on spatial coverage (e.g., requiring MHWs to occupy a fixed fraction of the basin). The EOF analysis of MHW intensity revealed two dominant modes of variability. The first mode, explaining 22% of the total variance, shows basin-wide MHWs with particularly strong signals in the Arabian Sea. This mode is linked to an anomalous high pressure over the North Indian Ocean and a corresponding low pressure in the Southern Hemisphere. This configuration weakens the climatological pressure gradient and hence the monsoon winds, which in turn suppresses evaporation (and hence reducing evaporative cooling) and cloud formation. As a result, shortwave radiation penetrates more effectively, warming the upper ocean and promoting MHWs (Figure 6). This mode is predominantly associated with the mature phase of El Niño, consistent with previous studies showing that El Niño influences Indian Ocean SSTs through the Indian Ocean Basin Mode, thereby preconditioning the basin for large-scale MHW development (Xie et al., 2009).

The second mode, accounting for 8% of the total variance, shows a dipole-like pattern where its positive phase is characterized by MHWs in the Bay of Bengal and suppressed activity in the Arabian Sea, while the negative phase exhibits the opposite pattern. The positive phase is driven by mechanisms similar to EOF mode 1, though the effects are more localized over the Bay of Bengal. In the negative phase, MHWs are concentrated over the western Indian Ocean, particularly near the Somali coast. In this case, the weakening of monsoon winds is also confined to the region, potentially reducing upwelling and the associated cooling, thereby allowing SSTs to rise. Interestingly, shortwave radiation appears to play a less dominant role in this mode compared to the others. The PC2+ is found to be more common during the La Niña years, whereas PC1 is found to be more common during El Niño years. In contrast, PC2- events show only a weak association with ENSO compared to PC1 and PC2+, with only a few occurring during the early phase of El Niño, whereas PC1 is primarily associated with the mature phase of El Niño. Importantly, while PC1 reflects basin-scale preconditioning associated with the mature phase of ENSO, its evolution is also modulated by intraseasonal monsoon variability, whereas $PC2^{+}$ more strongly captures MHW variability arising from the interaction between evolving ENSO states and MISO dynamics. In particular, PC2+ tends to occur during the developing phase of La Niña and also aligns with MISO phases 4–5. Analysis of MISO phase evolution around MHW onset further shows that PC1 and PC2+ MHWs are preferentially initiated during MISO Phases 3–4, when surface winds are weak and evaporative cooling is reduced. Elevated MHW frequency during Phases 4–5 reflects persistence driven by upper-ocean heat storage, even as surface forcing begins to recover. This suggests that MHWs represented by PC1 and PC2+ are not solely a response to large-scale background forcing, but are modulated by the combined influence of ENSO evolution and intraseasonal monsoon variability.

These different EOF modes also modulate monsoon rainfall in distinct ways. During the positive phases of PC1 and PC2, southern India tends to experience wetter conditions, while northern India becomes relatively drier, a rainfall distribution commonly associated with MISO phases 3–4. In contrast, PC2- is linked to widespread dryness across much of the Indian subcontinent. We also investigated the post-MHW rainfall response and found that the termination of PC1 events typically brings enhanced rainfall to northwest and northeast India, as well as to Bangladesh and Myanmar. In contrast, the end of PC2+ events is followed by increased rainfall over central India, while PC2- termination leads to enhanced rainfall over both south and central India. These delayed impacts are likely driven by the revival of monsoon winds following a break phase, which promotes the release of oceanic heat and moisture stored during the MHW event. These strengthened winds enhance evaporation over the ocean, as evidenced by negative latent heat flux anomalies, indicating heat transfer from ocean to atmosphere. The associated moisture flux contributes to increased cloud formation, which can further reduce incoming solar radiation, stabilizing the ocean surface and reinforcing the transition toward wetter atmospheric conditions.

Notably, we find that approximately one-third of PC1 and $PC2^{+}$ MHW events terminate during MISO Phase 6, a dynamically active phase characterized by strengthening monsoon circulation. Composites conditioned on MHW termination during this phase reveal systematic precipitation anomalies during MISO Phases 6 and 7 relative to MISO cycles without any MHW activity, indicating that MHW decay can actively modulate intraseasonal monsoon rainfall in addition to being shaped by MISO variability. This result provides evidence for a two-way coupling between MHWs and the MISO, in which intraseasonal monsoon dynamics regulate the lifecycle of MHWs, while MHW decay feeds back onto monsoon rainfall. Although these results indicate that MHW decay can actively modulate intraseasonal monsoon rainfall, a detailed investigation of the underlying physical mechanisms is beyond the scope of this study and remains an important direction for future work.

Our findings are consistent with the mechanisms highlighted by Roxy et al. (2017), who showed that SST warming in the Arabian Sea and the Bay of Bengal plays a critical role in fueling extreme rainfall events over central India. They traced nearly 36% of the total moisture during such events to the Arabian Sea, more than from the Bay of Bengal (26%) and central Indian Ocean (9%) combined. This underscores the importance of SST anomalies, such as those during MHWs, as a key moisture source. Additionally, a statistically significant increase in Arabian Sea moisture contribution has been observed over recent decades, suggesting a growing role for oceanic heat events like MHWs in intensifying monsoon extremes under climate change.

Overall, this study underscores the critical role of both the spatial structure and timing of MHWs in shaping monsoon variability. The results have significant implications for understanding and predicting regional rainfall extremes in a warming climate. Previous studies have shown that warming of the western Indian Ocean tends to reduce rainfall over the Indian subcontinent by weakening the land-sea pressure gradient and associated monsoon winds (Roxy et al.,

2015). In contrast, our results suggest that Indian Ocean warming, particularly through marine heatwaves, can enhance precipitation over parts of South Asia by increasing evaporation. Moreover, our findings suggest a possible interaction between MHWs, ENSO, and the MISO, raising important directions for future research. More broadly, our results point to a hierarchical coupling between large-scale climate modes and intraseasonal variability, in which ENSO sets the background thermodynamic state of the Indian Ocean, while the MISO modulates the timing, regional expression, and termination of marine heatwaves.

Several studies have shown that the air-sea interaction can influence the MISO precipitation (Roxy and Tanimoto, 2007; Ajayamohan et al., 2008; Wang et al., 2009; Lin et al., 2010; Sabeerali et al., 2014; Zhang L. et al., 2018). Therefore, key questions include: Do MHWs feed back onto MISO by modulating SST and atmospheric convection? Can MHWs alter the propagation speed or intensity of MISO phases? Do MHWs shift the canonical rainfall patterns associated with different MISO phases? Could they delay or accelerate MISO phase transitions? How do larger-scale modes such as ENSO and the IOD modulate the MISO-MHW relationship? While these questions lie beyond the scope of the present study, they open up new directions for advancing our understanding of ocean-atmosphere coupling and improving monsoon forecasting skill in a changing climate. In particular, since we define MHWs using detrended SST anomalies, future research could investigate whether similar MHW-MISO interactions persist when using raw SSTs that include long-term warming trends.

Taken together, our results suggest that marine heatwaves in the North Indian Ocean, as identified from detrended SST anomalies, represent dynamically evolving events shaped by ENSO-driven basin-scale preconditioning and intraseasonal monsoon variability, rather than simple manifestations of long-term warming.

Data availability statement

The original contributions presented in the study are included in the article/Supplementary material, further inquiries can be directed to the corresponding author.

Author contributions

LJ: Conceptualization, Data curation, Formal analysis, Investigation, Methodology, Supervision, Validation, Visualization, Writing – original draft. NS: Conceptualization, Methodology, Resources, Supervision, Validation, Writing – review & editing. SV: Conceptualization, Methodology, Validation, Writing – review & editing. DD: Conceptualization, Methodology, Supervision, Validation, Visualization, Writing – review & editing. RM: Conceptualization, Resources, Supervision, Validation, Writing – review & editing.

Funding

The author(s) declared that financial support was received for this work and/or its publication. This work was supported by the Natural Environment Research Council [Grant NE/S007210/1]. DD was supported by the IIT Bhubaneswar seed grant [Grant RP426].

Acknowledgments

The authors gratefully acknowledge Lijo Abraham Joseph for his valuable discussions and insights. This research also utilized JASMIN, the UK's collaborative data analysis facility.

Conflict of interest

The author(s) declared that this work was conducted in the absence of any commercial or financial relationships that could be construed as a potential conflict of interest.

Generative AI statement

The author(s) declared that generative AI was used in the creation of this manuscript. AI tools such as ChatGPT and Grammarly were occasionally and mindfully used to assist with writing refinement and Python code refinement. These tools were not used to generate scientific content, results, or interpretations. All content was reviewed by the author(s) for factual accuracy and originality.

Any alternative text (alt text) provided alongside figures in this article has been generated by Frontiers with the support of artificial intelligence and reasonable efforts have been made to ensure accuracy, including review by the authors wherever possible. If you identify any issues, please contact us.

Publisher's note

Supplementary material

The Supplementary Material for this article can be found online at: https://www.frontiersin.org/articles/10.3389/fclim.2026.1801667/full#supplementary-material

References

Abish, B., Cherchi, A., and Ratna, S. B. (2017). ENSO and the recent warming of the Indian Ocean. *Int. J. Climatol.* 38, 203–214. doi: 10.1002/joc.5170

Ajayamohan, R. S., Rao, S. A., and Yamagata, T. (2008). Influence of Indian Ocean dipole on poleward propagation of boreal summer intraseasonal oscillations. *J. Clim.* 21, 5437–5454. doi: 10.1175/2008JCLI1758.1

Albert, J., Gulakaram, V. S., Vissa, N. K., Bhaskaran, P. K., and Dash, M. K. (2023). Recent warming trends in the Arabian Sea: causative factors and physical mechanisms. *Climate* 11, 35–35. doi: 10.3390/cli11020035

Amaya, D. J., Jacox, M. G., Fewings, M. R., Saba, V. S., Stuecker, M. F., Rykaczewski, R. R., et al. (2023). Marine heatwaves need clear definitions so coastal communities can adapt. *Nature* 616, 29–32. doi: 10.1038/d41586-023-00924-2

Capotondi, A., Rodrigues, R. R., Sen Gupta, A., Benthuysen, J. A., Deser, C., Frölicher, T. L., et al. (2024). A global overview of marine heatwaves in a changing climate. *Commun. Earth Environ.* 5. doi: 10.1038/s43247-024-01806-9

Chakraborty, A., Chandrakar, R., Kumar, S., Sadhukhan, B., and Kumar, A. (2023). Analysis of marine heatwaves and biogeochemistry in the Northern Arabian Sea. *Reg. Stud. Mar. Sci.* 63:103019. doi: 10.1016/j.rsma.2023.103019

Chatterjee, A., Anil, G., and Shenoy, L. R. (2022). Marine heatwaves in the Arabian Sea. *Ocean Sci.* 18, 639–657. doi: 10.5194/os-18-639-2022

Cheng, Y., Zhang, M., Song, Z., Wang, G., Zhao, C., Shu, Q., et al. (2023). A quantitative analysis of marine heatwaves in response to rising sea surface temperature. *Sci. Total Environ.* 881:163396. doi: 10.1016/j.scitotenv.2023.163396

Dey, D., and Döös, K. (2021). Tracing the origin of the South Asian summer monsoon precipitation and its variability using a novel lagrangian framework. *J. Clim.* 34, 8655–8668. doi: 10.1175/JCLI-D-20-0967.1

D'Mello, J. R., and Kumar, S. P. (2018). Processes controlling the accelerated warming of the Arabian Sea. *Int. J. Climatol.* 38, 1074–1086. doi: 10.1002/joc.5198

Fu, X., Wang, B., Li, T., and McCreary, J. P. (2003). Coupling between northward-propagating, intraseasonal oscillations and sea surface temperature in the Indian Ocean. *J. Atmos. Sci.* 60, 1733–1753. doi: 10.1175/1520-0469(2003)060<1733:CBNIOA>2.0.CO;2

Fu, X., Wang, B., Waliser, D. E., and Tao, L. (2007). Impact of atmosphereocean coupling on the predictability of monsoon intraseasonal oscillations. *J. Atmos. Sci.* 64, 157–174. doi: 10.1175/JAS3830.1

Gao, X., Li, G., Liu, J., and Long, S.-M. (2022). The trend and interannual variability of marine heatwaves over the Bay of Bengal. *Atmosphere* 13:469. doi: 10.3390/atmos13030469

Good, S., Fiedler, E., Mao, C., Martin, M. J., Maycock, A., Reid, R., et al. (2020). The current configuration of the ostia system for operational production of foundation sea surface temperature and ice concentration analyses. *Remote Sens.* 12:720. doi: 10.3390/rs12040720

Goswami, B. N., and Mohan, R. S. A. (2001). Intraseasonal oscillations and interannual variability of the Indian summer monsoon. *J. Clim.* 14, 1180–1198. doi: 10.1175/1520-0442(2001)014<1180:IOAIVO>2.0.CO;2

Guo, F., Liu, Q., Yang, J., and Fan, L. (2017). Three types of Indian Ocean basin modes. *Clim. Dyn.* 51, 4357–4370. doi: 10.1007/s00382-017-3676-z

Gupta, H., Deogharia, R., Sil, S., and Dey, D. (2024). Characteristics of marine heat extreme evolution in the Northern Indian Ocean. *Int. J. Climatol.* 45. doi: 10.1002/joc.8734

Gupta, H., Sil, S., Gangopadhyay, A., and Gawarkiewicz, G. (2023). Observed surface and subsurface marine heat waves in the Bay of Bengal from *in-situ* and high-resolution satellite data. *Clim. Dyn.* 62, 203–221. doi: 10.1007/s00382-023-06913-5

Hersbach, H., Bell, B., Berrisford, P., Hirahara, S., Horányi, A., Mu noz-Sabater, J., et al. (2020). The ERA5 global reanalysis. *Q. J. R. Meteorol. Soc.* 146, 1999–2049. doi: 10.1002/qj.3803

Hobday, A. J., Alexander, L. V., Perkins, S. E., Smale, D. A., Straub, S. C., Oliver, E. C., et al. (2016). A hierarchical approach to defining marine heatwaves. *Prog. Oceanogr.* 141, 227–238. doi: 10.1016/j.pocean.2015.12.014

Jacox, M. G. (2019). Marine heatwaves in a changing climate. *Nature* 571, 485–487. doi: 10.1038/d41586-019-02196-1

Johnson, G. C., Lumpkin, R., Atkinson, C., Bil, T., Boyer, T., Bringas, F., et al. (2023). Global oceans. *Bull. Am. Meteorol. Soc.* 104, S146–S206. doi: 10.1175/BAMS-D-23-0076.2

Joseph, L., Dey, D., Skliris, N., Sanchez-Franks, A., Marsh, R., Hirschi, J., et al. (2026). Warming trend in the western Indian Ocean driven by oceanic transport. *J. Geophys. Res. Oceans* 131:e2025JC022762. doi: 10.1029/2025JC022762

Joseph, L., Skliris, N., Dey, D., Marsh, R., and Hirschi, J. (2024). Increased summer monsoon rainfall over northwest india caused by hadley cell expansion and Indian Ocean warming. *Geophys. Res. Lett.* 51:e2024GL108829. doi: 10.1029/2024GL108829

Kemball-Cook, S., and Wang, B. (2001). Equatorial waves and airsea interaction in the boreal summer intraseasonal oscillation. *J. Clim.* 14, 2923–2942. doi: 10.1175/1520-0442(2001)014<2923:EWAASI>2.0.CO;2

Klein, S. A., Soden, B. J., and Lau, N.-C. (1999). Remote sea surface temperature variations during enso: evidence for a tropical atmospheric bridge. *J. Clim.* 12, 917–932. doi: 10.1175/1520-0442(1999)012<0917:RSSTVD>2.0.CO;2

Koul, V., Brune, S., Akimova, A., Düsterhus, A., Pieper, P., Hövel, L., et al. (2023). Seasonal prediction of Arabian Sea marine heatwaves. *Geophys. Res. Lett.* 50:e2023GL103975. doi: 10.1029/2023GL103975

Krishnamurthy, V., and Kirtman, B. P. (2009). Relation between indian monsoon variability and SST. *J. Clim.* 22, 4437–4458. doi: 10.1175/2009JCLI2520.1

Kumar, S., Chakraborty, A., Chandrakar, R., Kumar, A., Sadhukhan, B., and Roy Chowdhury, R. (2023). Analysis of marine heatwaves over the Bay of Bengal during 1982–2021. *Sci. Rep.* 13:14235. doi: 10.1038/s41598-023-43101-1

Liang, K., Qiu, Y., Lin, X., Lin, W., Ni, X., and He, Y. (2024). An increase in autumn marine heatwaves caused by the Indian Ocean dipole in the Bay of Bengal. *J. Clim.* 37, 4523–4539. doi: 10.1175/JCLI-D-23-0541.1

Lin, A., Li, T., Fu, X., Luo, J.-J., and Masumoto, Y. (2010). Effects of airsea coupling on the boreal summer intraseasonal oscillations over the tropical Indian Ocean. *Clim. Dyn.* 37, 2303–2322. doi: 10.1007/s00382-010-0943-7

Mathew, S., Natesan, U., Latha, G., and Venkatesan, R. (2018). Dynamics behind warming of the Southeastern Arabian Sea and its interruption based on *in situ* measurements. *Ocean Dyn.* 68, 457–467. doi: 10.1007/s10236-018-1130-3

McMonigal, K., Gunn, K. L., Beal, L. M., Elipot, S., and Willis, J. K. (2022). Reduction in meridional heat export contributes to recent Indian Ocean warming. *J. Phys. Oceanogr.* 52, 329–345. doi: 10.1175/JPO-D-21-0085.1

Nisha, P., Pranesha, T., Vidya, P., Ravichandran, M., and Murtugudde, R. (2023). Trend and interannual variability of the Arabian Sea heat content. *J. Mar. Syst.* 242:103935. doi: 10.1016/j.jmarsys.2023.103935

Oliver, E. C. J., Donat, M. G., Burrows, M. T., Moore, P. J., Smale, D. A., Alexander, L. V., et al. (2018). Longer and more frequent marine heatwaves over the past century. *Nat. Commun.* 9:1324. doi: 10.1038/s41467-018-03732-9

Oppo, D. W., and Rosenthal, Y. (2010). The great indo-pacific communicator. *Science* 328, 1492–1494. doi: 10.1126/science.1187273

Prajeesh, A. G., Swapna, P., Krishnan, R., Ayantika, D. C., Sandeep, N., Manmeet, S., et al. (2021). The Indian summer monsoon and Indian Ocean dipole connection in the IITM earth system model (iitm-esm). *Clim. Dyn.* 58, 1877–1897. doi: 10.1007/s00382-021-05999-z

Pratik, K., Parekh, A., Karmakar, A., Chowdary, J. S., and Gnanaseelan, C. (2018). Recent changes in the summer monsoon circulation and their impact on dynamics and thermodynamics of the Arabian Sea. *Theoret. Appl. Climatol.* 136, 321–331. doi: 10.1007/s00704-018-2493-6

Rajeevan, M., Gadgil, S., and Bhate, J. (2010). Active and break spells of the Indian summer monsoon. *J. Earth Syst. Sci.* 119, 229–247. doi: 10.1007/s12040-010-0019-4

Rayner, N. A., Parker, D. E., Horton, E. B., Folland, C. K., Alexander, L. V., Rowell, D. P., et al. (2003). Global analyses of sea surface temperature, sea ice, and night marine air temperature since the late nineteenth century. *J. Geophys. Res.: Atmos.* 108. doi: 10.1029/2002JD002670

Reynolds, R. W., Rayner, N. A., Smith, T. M., Stokes, D. C., and Wang, W. (2002). An improved *in situ* and satellite SST analysis for climate. *J. Clim.* 15, 1609–1625. doi: 10.1175/1520-0442(2002)015<1609:AIISAS>2.0.CO;2

Rohde, R. (2025). *Global Temperature Report for 2024.* Available online at: https://berkeleyearth.org/global-temperature-report-for-2024/ (Accessed May 21, 2025).

Rosselló, P., Pascual, A., and Combes, V. (2023). Assessing marine heat waves in the Mediterranean Sea: a comparison of fixed and moving baseline methods. *Front. Mar. Sci.* 10:1168368. doi: 10.3389/fmars.2023.1168368

Roxy, M., and Tanimoto, Y. (2007). Role of sst over the Indian Ocean in influencing the intraseasonal variability of the Indian summer monsoon. *J. Meteorol. Soc. Jpn. Ser. II* 85, 349–358. doi: 10.2151/jmsj.85.349

Roxy, M. K., Ghosh, S., Pathak, A., Athulya, R., Mujumdar, M., Murtugudde, R., et al. (2017). A threefold rise in widespread extreme rain events over Central India. *Nat. Commun.* 8:708. doi: 10.1038/s41467-017-00744-9

Roxy, M. K., Ritika, K., Terray, P., and Masson, S. (2014). The curious case of Indian Ocean warming. *J. Clim.* 27, 8501–8509. doi: 10.1175/JCLI-D-14-00471.1

Roxy, M. K., Ritika, K., Terray, P., Murtugudde, R., Ashok, K., and Goswami, B. N. (2015). Drying of Indian subcontinent by rapid Indian Ocean warming and a weakening land-sea thermal gradient. *Nat. Commun.* 6:7423. doi: 10.1038/ncomms8423

Roxy, M. K., Saranya, J. S., Modi, A., Anusree, A., Cai, W., Resplandy, L., et al. (2024). "Future projections for the tropical Indian Ocean," in *The Indian Ocean and its Role in the Global Climate System*, eds. C. C. Ummenhofer and R. R. Hood (Amsterdam: Elsevier), 469–482. doi: 10.1016/B978-0-12-822698-8.00004-4

Sabeerali, C. T., Rao, S. A., George, G., Rao, D. N., Mahapatra, S., Kulkarni, A., et al. (2014). Modulation of monsoon intraseasonal oscillations in the recent warming period. *J. Geophys. Res.: Atmos.* 119, 5185–5203. doi: 10.1002/2013JD021261

Sajidh, C. K., Chatterjee, A., Murtugudde, R., McPhaden, M. J., Shenoi, S. S. C., and Vinayachandran, P. N. (2026). Rapid 21st century warming in the southern subtropical Indian Ocean driven by altered inter-basin connections. *Int. J. Climatol.* 46:e70157. doi: 10.1002/joc.70157

Sandaruwan, J. W. N. D., Zhou, W., Cheung, P. K. Y., Du, Y., and Wang, X. (2023). Characteristics and formation of two leading marine heatwave modes in the north Indian Ocean during summer and their implications for local precipitation. *J. Clim.* 36, 3385–3402. doi: 10.1175/JCLI-D-22-0574.1

Saranya, J. S., Roxy, M. K., Dasgupta, P., and Anand, A. (2022). Genesis and trends in marine heatwaves over the Tropical Indian Ocean and their interaction with the Indian summer monsoon. *J. Geophys. Res. Oceans* 127:e2021JC017427. doi: 10.1029/2021JC017427

Shee, A., Sil, S., and Gangopadhyay, A. (2023). Recent changes in the upper oceanic water masses over the Indian ocean using argo data. *Sci. Rep.* 13:20252. doi: 10.1038/s41598-023-47658-9

Skliris, N., Marsh, R., Haigh, I. D., Wood, M., Hirschi, J., Darby, S., et al. (2022). Drivers of rainfall trends in and around mainland Southeast Asia. *Front. Clim.* 4:926568. doi: 10.3389/fclim.2022.926568

Suhas, E., Neena, J. M., and Goswami, B. N. (2012). An indian monsoon intraseasonal oscillations (miso) index for real time monitoring and forecast verification. *Clim. Dyn.* 40, 2605–2616. doi: 10.1007/s00382-012-1462-5

Swapna, P., Krishnan, R., and Wallace, J. M. (2013). Indian ocean and monsoon coupled interactions in a warming environment. *Clim. Dyn.* 42, 2439–2454. doi: 10.1007/s00382-013-1787-8

Swetha, S., Ramesh, K. V., and Rakesh, V. (2025). Influence of large-scale climate modes (ENSO, IOD and PJ) on marine heatwave characteristics in the Indian Ocean region. *Theoret. Appl. Climatol.* 156. doi: 10.1007/s00704-025-05570-4

Titchner, H. A., and Rayner, N. A. (2014). The met office hadley centre sea ice and sea surface temperature data set, version 2: 1. sea ice concentrations: Hadisst.2.1.0.0 sea ice concentrations. *J. Geophys. Res.: Atmos.* 119, 2864–2889. doi: 10.1002/2013JD020316

Vecchi, G. A., and Harrison, D. E. (2002). Monsoon breaks and subseasonal sea surface temperature variability in the bay of bengal. *J. Clim.* 15, 1485–1493. doi: 10.1175/1520-0442(2002)015<1485:MBASSS>2.0.CO;2

Venegas, R. M., Acevedo, J., and Treml, E. A. (2023). Three decades of ocean warming impacts on marine ecosystems: a review and perspective. *Deep Sea Res. Part II: Top. Stud. Oceanogr.* 212:105318. doi: 10.1016/j.dsr2.2023.105318

Wang, W., Chen, M., and Kumar, A. (2009). Impacts of ocean surface on the northward propagation of the boreal summer intraseasonal oscillation in the ncep climate forecast system. *J. Clim.* 22, 6561–6576. doi: 10.1175/2009JCLI3007.1

World Meteorological Organization (2025). *State of the Climate 2024: Update for cop29*. Available online at: https://library.wmo.int/idurl/4/69075 (Accessed May 21, 2025).

Xie, S.-P., Hu, K., Hafner, J., Tokinaga, H., Du, Y., Huang, G., et al. (2009). Indian Ocean capacitor effect on indowestern pacific climate during the summer following el niño. *J. Clim.* 22, 730–747. doi: 10.1175/2008JCLI2544.1

Yadav, R. K., and Roxy, M. K. (2019). On the relationship between north India summer monsoon rainfall and east equatorial Indian Ocean warming. *Glob. Planet. Change* 179:23–32. doi: 10.1016/j.gloplacha.2019.05.001

Yang, J., Liu, Q., Xie, S., Liu, Z., and Wu, L. (2007). Impact of the Indian Ocean sst basin mode on the Asian summer monsoon. *Geophys. Res. Lett.* 34. doi: 10.1029/2006GL028571

Zhang, L., Han, W., Li, Y., and Maloney, E. D. (2018). Role of north Indian Ocean airsea interaction in summer monsoon intraseasonal oscillation. *J. Clim.* 31, 7885–7908. doi: 10.1175/JCLI-D-17-0691.1

Zhang, Y., Zhang, Y., Feng, M., Feng, M., Du, Y., Phillips, H. E., et al. (2018). Strengthened indonesian throughflow drives decadal warming in the Southern Indian Ocean. *Geophys. Res. Lett.* 45, 6167–6175. doi: 10.1029/2018GL078265